



# MIT Open Access Articles

## *An unreleased mm-wave resonant body transistor*

The MIT Faculty has made this article openly available. **Please share** how this access benefits you. Your story matters.

<b>Citation</b>	Wang, Wentao et al. "An Unreleased Mm-wave Resonant Body Transistor." IEEE 24th International Conference on Micro Electro Mechanical Systems (MEMS), 2011. 1341–1344.
<b>As Published</b>	<a href="http://dx.doi.org/10.1109/MEMSYS.2011.5734682">http://dx.doi.org/10.1109/MEMSYS.2011.5734682</a>
<b>Publisher</b>	Institute of Electrical and Electronics Engineers (IEEE)
<b>Version</b>	Author's final manuscript
<b>Accessed</b>	Thu Apr 19 09:25:54 EDT 2018
<b>Citable Link</b>	<a href="http://hdl.handle.net/1721.1/73576">http://hdl.handle.net/1721.1/73576</a>
<b>Terms of Use</b>	Creative Commons Attribution-Noncommercial-Share Alike 3.0
<b>Detailed Terms</b>	<a href="http://creativecommons.org/licenses/by-nc-sa/3.0/">http://creativecommons.org/licenses/by-nc-sa/3.0/</a>

# AN UNRELEASED MM-WAVE RESONANT BODY TRANSISTOR

Wentao Wang, Laura C. Popa, Radhika Marathe, Dana Weinstein  
Massachusetts Institute of Technology, Cambridge, MA, USA

## ABSTRACT

In this work, we present the first fully unreleased Micro-Electro-Mechanical (MEM) resonator. The 1<sup>st</sup> harmonic longitudinal resonance of a silicon FinFET fully clad in SiO<sub>2</sub> is demonstrated. The device exhibits two resonances at 39 and 41 GHz, corresponding well with simulation results. The quality factor ( $Q$ ) of 129 at 39 GHz is  $\sim 4\times$  lower than that of its released counterpart. Methods to improve  $Q$  and reduce spurious modes are introduced. This first demonstration of unreleased resonators in a hybrid MEMS-CMOS technology can provide RF and microwave CMOS circuit designers with active high- $Q$  devices monolithically integrated in Front-End-of-Line (FEOL) processing without the need for post-processing or special packaging.

## INTRODUCTION

Two of the greatest challenges currently faced by MEMS are those of packaging and integration with CMOS technology. Motivation for monolithic integration includes enhanced signal transduction, reduced footprint, improved immunity from parasitics and electromagnetic interference, and potentially lower cost compared to multichip systems. Methods for MEMS-CMOS cofabrication have focused on modular MEMS-first or MEMS-last processes. However, the increased mask count of these processes decreases yield and increases cost due to added complexity. Moreover, the constraints on the process sequence, thermal budget, and materials require a compromise between the MEMS and electronic devices and lead to reduced performance [1]. Non-modular MEMS-CMOS processing has been demonstrated using the Back-End-of-Line (BEOL) CMOS stack, reducing mask count but limiting MEMS materials to metals and dielectrics. This method also requires a post-processing release step to suspend the structure [2].

The need for direct integration of MEMS devices with CMOS is critical for successful implementation of high frequency active MEM resonators. Monolithic integration of these devices can provide basic RF and mm-wave building blocks with high  $Q$ , small footprint, and low power for use in wireless communication, microprocessor clocking, navigation and sensing applications. Nevertheless, the majority of MEM resonators require a release step to freely suspend the moving structures. This necessitates complex encapsulation and packaging, restricting fabrication to MEMS-last or BEOL processing of large-scale devices.

To overcome these obstacles, this paper reports on the first fully unreleased MEM resonator, comprising a Resonant Body Transistor (RBT) at 39 GHz, bound on all sides by a thick SiO<sub>2</sub> layer (Figure 1). This resonator demonstrates the feasibility of direct integration into FEOL CMOS processing, making these devices an attractive

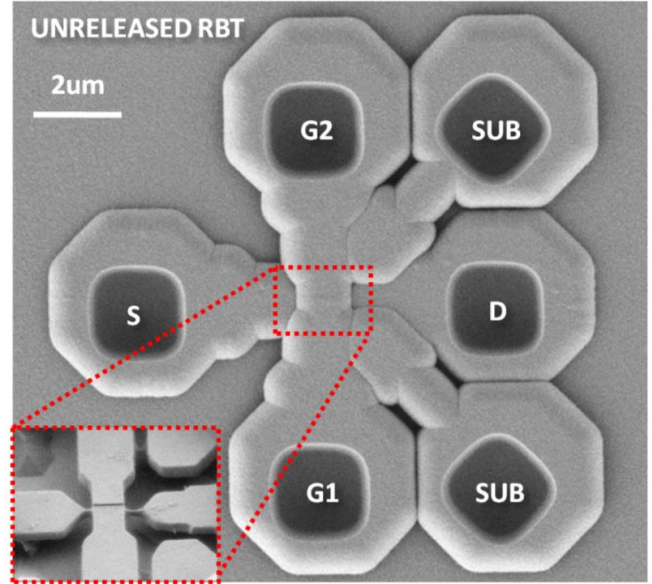


**Figure 1:** Scanning electron micrograph (SEM) of the unreleased RBT. The 1  $\mu\text{m}$  thick field oxide is visible on top of the unreleased resonator, showing contact holes to the silicon underneath. (Inset) Device with oxide cladding removed to show the underlying RBT.

choice for low power clock generation and high- $Q$  tank circuits.

Solid-mount Bulk Acoustic Wave (BAW) resonators have previously been demonstrated, using acoustic Bragg reflectors to isolate vibrations from the substrate underneath [3]. While these devices do not require any release step, they depend on free boundary conditions on 5 of 6 sides to operate. This necessitates special packaging and restricts solid-mount devices to MEMS-last design.

The authors have previously demonstrated RBTs with internal dielectric drive and Field Effect Transistor (FET) sensing up to 37 GHz [4,5]. Fabrication of these RBTs is very similar to that of independent-gate FinFETs, and enables amplification of the mechanical signal before the presence of electrical parasitics, allowing detection up to mm-wave frequencies.

The unreleased resonator demonstrated here is not limited to CMOS processes, and can be implemented in applications where a minimal or no-packaging solution is needed.

## RBT PRINCIPLE OF OPERATION

Unlike capacitive sensing employed in traditional electrostatic resonators, FET sensing can be used to amplify the mechanical signal prior to any feed-through parasitics. Combining the benefits of FET sensing with the frequency scaling and high- $Q$  capabilities of internal dielectrically

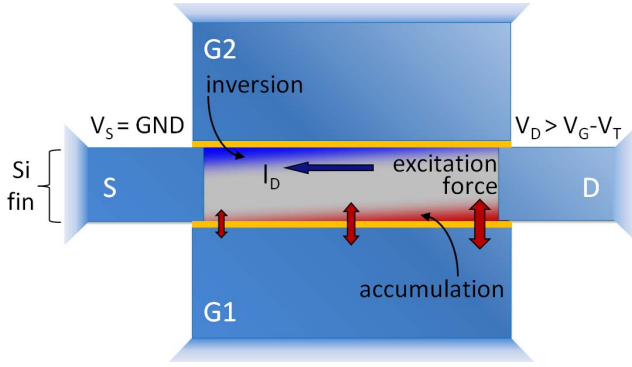


**Figure 2:** Top-view schematic showing principle of operation of a bulk-mode dielectrically transduced Resonant Body Transistor. The accumulation gate (G1) capacitively drives longitudinal waves in the fin while a FET channel generated by the inversion gate (G2) piezoresistively senses resonance.

transduced resonators [6], RBTs can achieve frequencies of operation previously inaccessible in silicon.

Figure 2 shows a top-view schematic of the RBT principle of operation. The region in light grey represents the undoped active area of the FET, while the blue region is highly doped. The active area near the drive electrode G1 is biased into accumulation (red), so that a capacitive force acts across the thin dielectric film (yellow) driving longitudinal waves in the fin. A DC gate voltage is applied to G2, generating an inversion channel (blue) which results in a DC drain current. At resonance, elastic waves modulate the drain current by the piezoresistive effect. The gain of the transistor reduces the output impedance of the device, providing high transduction efficiency at RF and mm-wave frequencies.

RBTs were fabricated in an SOI process similar to that of independent-gate FinFETs, as described in [4]. An SEM of the unreleased RBT (before metallization) is found in Figure 1, showing the field oxide (FOX) layer on top of the device with silicided holes for electrical contact to the silicon device layer underneath. The inset of Figure 1 depicts the device with oxide cladding removed to show the underlying RBT.

The operation of the RBT can be described by modifying the small signal model of a traditional field effect transistor, as shown in Figure 3. Analogous to the FET equivalent circuit, the model includes transconductance terms  $g_m$  and  $g_{mb}$  of front and back gate respectively, defining the electronic amplification of the RBT. In addition, a mechanical transconductance  $g_{ma}$  is introduced to express the electromechanical amplification of the mechanical signal which exhibits a Lorentzian frequency response, with center frequency and quality factor defined by acoustic resonance. Under DC biasing condition of the inversion gate G2, the small signal current due to the front gate ( $g_m v_{gs}$ ) is suppressed. Additionally, the current due to  $g_{mb}$  is engineered to be small, particularly in standard CMOS technology. The dominant AC signal is attributed to the electromechanical  $g_{ma}$ . The derivation for the piezoresistive

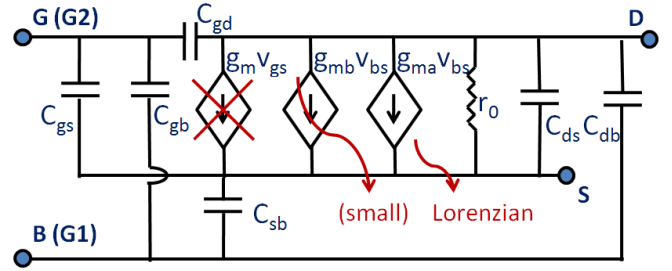


**Figure 3:** Small signal model of the RBT.  $g_m$  is the transistor transconductance through the front gate G2, and  $g_{mb}$  is that of back gate G1. Current due to the front gate is suppressed by DC biasing. The back gate effect is small, and defines the signal floor. The Lorentzian frequency response of the piezoresistive transconductance  $g_{ma}$  describes the high-Q electromechanical amplification at resonance.

transconductance  $g_{ma} = 1/R_{X,RBT}$  is provided in [4], showing a direct dependence on the  $g_m$  of the FET. The dynamic range of the RBT is therefore limited by the back gate contribution to the drain current modulation and by the inherent electrical gain of the transistor. The FET  $g_m$  is also the primary limitation in frequency scaling of the resonator, as the drain current modulation cannot be measured reliably beyond the transistor's cutoff frequency  $f_T$ . The performance of these active MEM resonators is therefore defined by the quality of transistor technology, and can benefit greatly from direct integration with cutting edge CMOS circuits.

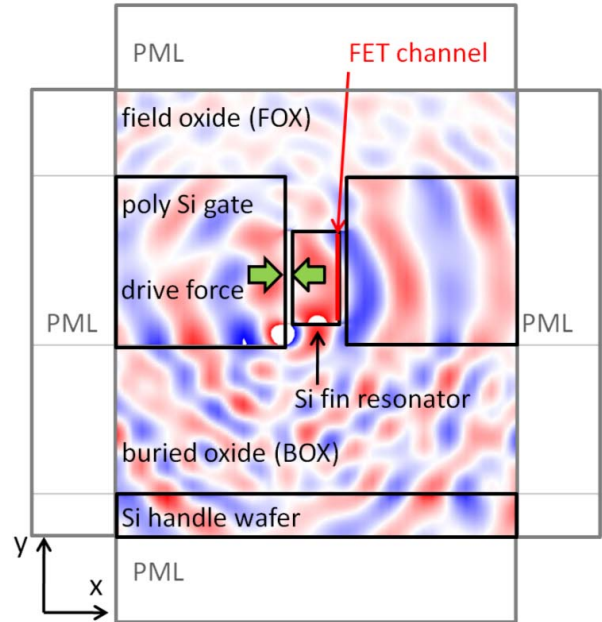


**Figure 4:** COMSOL simulation of side view of unreleased resonant mode in RBT, showing contour plot of stress along x-axis. A force applied across one dielectric (15 nm silicon nitride) generates a 1<sup>st</sup> harmonic longitudinal mode detected by strain induced in the FET channel. PMLs indicate regions of no reflected energy.

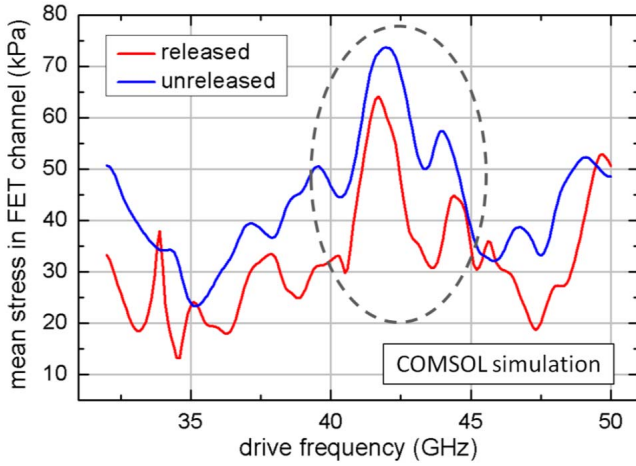


**Figure 5:** Simulated frequency response of unreleased resonator showing resonance for both released and unreleased devices at the targeted frequency.

## SIMULATION OF FULLY UNRELEASED RESONATORS

COMSOL simulations of both released and unreleased (fully-clad) RBTs were performed to determine the distortion of the 1st harmonic longitudinal resonance in the presence of buried oxide (340 nm BOX) under the device and field oxide (1  $\mu\text{m}$  FOX) above it (Figure 4). The single crystal silicon fin in the simulation is of 114 nm width (x-direction) and 220 nm thickness (y-direction), with 15 nm  $\text{Si}_3\text{N}_4$  gate dielectrics and poly silicon gates of 400 nm width and 400 nm thickness. In addition, due to etching of the BOX during an over-etch of the device layer, the fin was offset by 50 nm from the bottom of the poly gate according to fabrication data. Longitudinal waves are excited at the accumulation gate dielectric and sensed piezoresistively at the FET channel. The dielectric on the left was loaded by a pair of equal and opposite external forces to represent the capacitive driving force. Meanwhile, the stress at the interface between the fin and the dielectric on the right was integrated to generate the output signal, indicating the strength of piezoresistive modulation on the drain current.

A frequency sweep from 30 to 50 GHz was performed in frequency response analysis in COMSOL structural mechanics module, shown in Figure 5. Resonance peaks were observed at 42 and 44 GHz for both released and unreleased RBTs. The similarity in frequency response between the released and unreleased devices indicates the capacity to design and realize bulk-mode unreleased resonators at RF and mm-wave frequencies.

## EXPERIMENTAL RESULTS

The unreleased RBTs were tested in a standard two-port configuration at room temperature in a vacuum probe station, as described in [5]. Vacuum measurement was only necessary to prevent oxidation of the Ni metallization, and does not affect device performance.

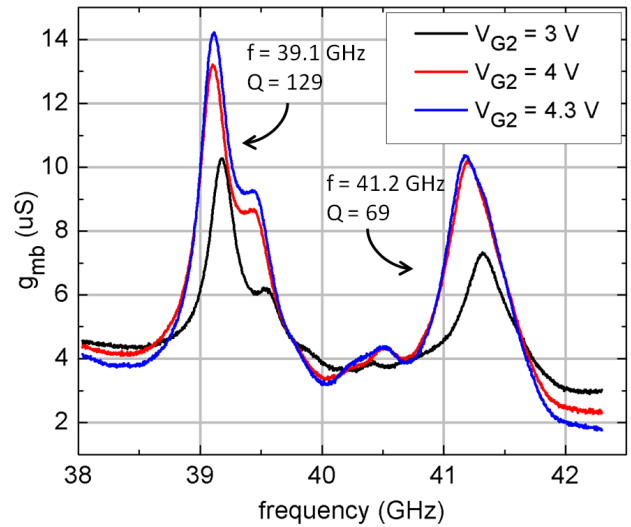


**Figure 6:** Measured frequency response of the unreleased RBT after standard short-open de-embedding.

The measured frequency response of the unreleased RBT is given in Figure 6. The DC bias of inversion gate  $V_{G2}$  was set at 3 V, 4 V, and 4.3 V successively, with a DC accumulation gate voltage  $V_{G1}$  of -1.12 V, drain voltage  $V_D$  of 4.31 V, and an input RF power of -13 dBm. The device exhibits two peaks at 39 and 41 GHz, corresponding well with simulation results. The slight shift in resonance frequency compared to simulation can be attributed to variation of fin length and damping mechanisms. The  $Q$  of 129 at 39 GHz ( $f \cdot Q$  product of  $5 \times 10^{12}$ ) is  $\sim 4\times$  lower than that of its released counterpart [5]. Both  $Q$  and spurious modes can be improved by patterning the gates of the device. This was not possible due to routing limitations of the coplanar fabrication process, but is easily achievable with vias of the standard CMOS metal stack.

The signal increase with sensing gate voltage demonstrates signal amplification due to increasing transconductance  $g_m$  of the FET, and validates that the signal originates from mechanical resonance. With the increase of  $V_{G2}$  from 3 V to 4.3 V, the resonance frequency shifts by 0.1 GHz and 0.2 GHz for 39 GHz and 41 GHz peaks respectively. The observed frequency shift results from local resistive heating due to increased DC drain current at higher gate voltage, which alters the Young's modulus of silicon. Engineering of the temperature coefficient of frequency (TCF) has been demonstrated using composite Si-SiO<sub>2</sub> resonators to reduce temperature sensitivity well below 1 ppm/ $^{\circ}\text{C}$  [7]. Similarly, the TCF of this unreleased resonator can be compensated and reduced by adjusting the oxide thickness, making the resonator temperature insensitive. In a technology with limited control over layer thickness, this can be achieved by strategically patterning material around the resonant structure.

## CONCLUSION

The 1st harmonic longitudinal resonance of a silicon bar Resonant Body Transistor, fully clad in SiO<sub>2</sub>, was



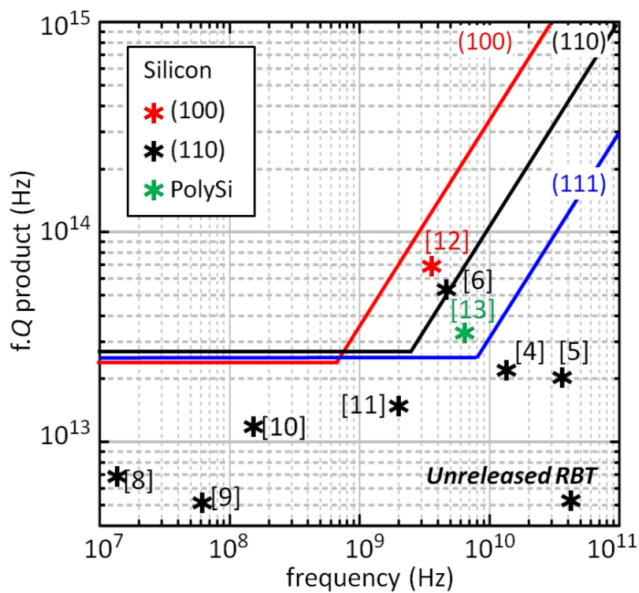


**Figure 7:** Frequency-quality factor products of various silicon-based electrostatic resonators, plotted against the theoretical limit of phonon-phonon scattering.

demonstrated at 39 GHz with a quality factor of 129. The resulting  $f.Q$  product of  $5 \times 10^{12}$  is plotted in Figure 7 against the fundamental limit of silicon defined by phonon-phonon scattering. At high frequencies in the Landau-Rumer regime [14], resonator  $Q$  is limited primarily by anchor loss where the acoustic wavelength is comparable to and can be smaller than the dimensions of the supporting structure.

Anchor loss in released resonant cavities at GHz frequencies has been addressed by use of phononic crystals surrounding the device [15]. This method has been shown to approach the phonon-phonon scattering limit in this frequency range. The quality factor of *unreleased resonators* can be significantly improved by localization of acoustic energy using acoustic Bragg reflectors [3] or phononic crystals. These designs can provide near-perfect acoustic mirrors in place of the lossy support beams required for released resonators. At mm-wave frequencies, unreleased resonators with energy localization may therefore achieve better performance than their released counterparts.

Fabrication of the RBTs demonstrated in this work is very similar to that of independent-gate FinFETs, and enables amplification of the mechanical signal before the presence of electrical parasitics. This first demonstration of an unreleased resonator in a hybrid MEMS-CMOS technology can provide RF and microwave CMOS circuit designers with active high- $Q$  devices monolithically integrated without the need for post-processing or special packaging.

## ACKNOWLEDGEMENTS

This work was funded by the MARCO Center for Materials, Structures and Devices (MSD) and by the DARPA Young Faculty Award. Devices were fabricated at

the Cornell Nanoscale Science and Technology Facility (CNF). The authors thank Sony Corporation for their valuable support.

## REFERENCES

- [1] G.K. Fedder, R.T. Howe, T.-J. King Liu, E.P. Quevy, "Technologies for cofabricating MEMS and electronics," *Proceedings of the IEEE*, **96** (2), 306-322 (2008).
- [2] F. H. Xie, L. Erdmann, X. Zhu, K. Gabriel, G.K. Fedder, "Post-CMOS processing for high-aspect-ratio integrated silicon microstructures," *J. Microelectromech. Syst.* **11** (2), 93-101 (2002).
- [3] S. Marksteiner, J. Kaitila, G. Fattinger, R. Aigner, "Optimization of acoustic mirrors for solidly mounted BAW resonators," *IEEE Ultrasonic Symposium 2005*, 329-332 (2005).
- [4] D. Weinstein, S.A. Bhawe, "The resonant body transistor" *Nano Letters* **10** (4), 1234-1237 (2010).
- [5] D. Weinstein, S.A. Bhawe, "Acoustic resonance in an independent-gate FinFET," *Hilton Head 2010*, 459-462 (2010).
- [6] D. Weinstein, S.A. Bhawe, "Internal dielectric transduction of a 4.5 GHz silicon bar resonator," *IEEE IEDM 2007*, 415-418 (2007).
- [7] R. Melamud, S.A. Chandorkar, B. Kim, H.K. Lee, J.C. Salvia, G. Bahl, M.A. Hopcroft, T.W. Kenny, "Temperature-insensitive composite micromechanical resonators," *J. Microelectromech. Syst.* **18** (6), 1409-1419 (2009).
- [8] L. Khine, M. Palaniapan, W.-K. Wong, "6MHz bulk-mode resonator with  $Q$  values exceeding one million," *Transducers 2007*, 2445-2448 (2007).
- [9] Y.-W. Lin, S. Lee, S.-S. Li, Y. Xie, Z. Ren, C.T.-C. Nguyen, "Series-resonant VHF micromechanical resonator reference oscillators," *J. Solid State Circuits* **39** (12), 2477-2491 (2004).
- [10] H.M. Lavasani, A.K. Samaroo, G. Casinovi, F. Ayazi, "A 145MHz low phase-noise capacitive silicon micromechanical oscillator," *IEDM 2008*, 675-678 (2008).
- [11] M. Ziaei-Moayyed, J. Hsieh, J.-W.P. Chen, E.P. Quevy, D. Elata, R.T. Howe, "Higher-order mode internal electrostatic transduction of a bulk-mode ring resonator on a quartz substrate," *Transducers 2009*, 2338-2341 (2010).
- [12] E. Hwang, S.A. Bhawe, "PN-diode transduced 3.7 GHz silicon resonator," *MEMS 2010*, 208-211 (2010).
- [13] D. Weinstein, S.A. Bhawe, "Frequency scaling and transducer efficiency in internal dielectrically transduced silicon bar resonators," *Transducers 2009*, 708-711 (2009).
- [14] R. Tabrizian, M. Rais-Zadeh, F. Ayazi, "Effect of phonon interactions on limiting the  $f.Q$  product of micromechanical resonators," *Transducers 2009*, 2131-2134 (2009).
- [15] D. Goettler, M. Su, Z. Leseman, Y. Soliman, R. Olsson, I. El-Kady, "Realizing the frequency quality factor product limit in silicon via compact phononic crystal resonators," *J. App. Phys.* **108**, 084505 (2010).